The Astrophysical Journal, 737:21 (14pp), 2011 August 10 doi:10.1088/0004-637X/737/1/21

NUMERICAL CALCULATION OF MAGNETOBREMSSTRAHLUNG EMISSION AND ABSORPTION COEFFICIENTS

Po Kin Leung[1], Charles F. Gammie[2,3], and Scott C. Noble[4]
[1] Department of Physics, University of California, Santa Barbara, CA 93106, USA; pkleung@physics.ucsb.edu
[2] Astronomy Department, University of Illinois, Urbana, IL 61801, USA
[3] Physics Department, University of Illinois, Urbana, IL 61801, USA; gammie@illinois.edu
[4] Center for Computational Relativity and Gravitation, School of Mathematical Sciences, Rochester Institute of Technology, Rochester, NY 14623, USA; scn@astro.rit.edu
Received 2009 October 29; accepted 2011 May 13; published 2011 July 26

ABSTRACT

Magnetobremsstrahlung (MBS) emission and absorption play a role in many astronomical systems. We describe a general numerical scheme for evaluating MBS emission and absorption coefficients for both polarized and unpolarized light in a plasma with a general distribution function. Along the way we provide an accurate scheme for evaluating Bessel functions of high order. We use our scheme to evaluate the accuracy of earlier fitting formulae and approximations. We also provide an accurate fitting formula for mildly relativistic ($kT/(m_e c^2) \gtrsim 0.5$) thermal electron emission (and therefore absorption). Our scheme is too slow, at present, for direct use in radiative transfer calculations but will be useful for anyone seeking to fit emission or absorption coefficients in a particular regime.

Key words: methods: numerical – radiation mechanisms: general

Online-only material: color figures

1. INTRODUCTION

In many astronomical plasmas the electron distribution includes an approximately thermal, mildly relativistic component. As theoretical models of such systems advance, it is useful to have a fast, accurate scheme to calculate the magnetobremsstrahlung (MBS), or cyclo-synchrotron, spectra. It is particularly desirable to be able to evaluate the necessary absorption and emission coefficients for polarized radiation from a general electron distribution, since in the collisionless conditions common in low luminosity active galactic nuclei electron distributions are unlikely to precisely follow the commonly assumed thermal or power-law forms.

Usually MBS spectra are calculated using emission and absorption coefficients derived under an ultrarelativistic (synchrotron) approximation or, for mildly relativistic electrons, using approximate fitting formulae. The fitting formulae are accurate over a limited range in frequency ν, field strength B, observer angle θ (the angle between the emitted or absorbed photon and the magnetic field vector $\mathbf{B}$), or characteristic Lorentz factor for the electrons. In this work we provide, test, and apply a general scheme for calculating MBS emission and absorption coefficients. One potential application of our methods is to generate new, more accurate, and computationally efficient fitting formulae over the range of interest.

Approximate calculations of MBS emission and absorption coefficients have a rich history. In the ultrarelativistic limit, emission of an electron with Lorentz factor γ is limited to a cone defined by the oscillating velocity vector of the electron, with angular width $1/\gamma$. This leads to an approximate expression for $dP/d\nu$ (Westfold 1959; Bekefi 1966; Rybicki & Lightman 1979), the power per unit frequency interval. However, for $\gamma \sim 1$, the approximation worsens, cyclotron line features begin to appear in the spectrum, and the ultrarelativistic approximation must be abandoned.

For mildly relativistic electrons the emission is still mainly perpendicular to the magnetic field. This fact can be used to develop approximate analytic expressions for the emissivity. Petrosian (1981) used the method of steepest descent, and an asymptotic expansion of the Bessel functions, to find the emissivity of mildly relativistic thermal electrons (see also Pacholczyk 1970).

Robinson & Melrose (1984) and Dulk (1985) improved Petrosian's (1981) calculation for thermal electrons at temperature T by using more accurate asymptotic expansions of the Bessel functions that appear in the exact expression for the emissivity, and some interpolation formulae, to provide a thermal MBS emissivity that is valid over a wide range in T, ν, θ, and B. Brainerd & Lamb (1987) numerically calculate emissivity for various distributions and energy injection functions. Brainerd & Petrosian (1987) calculate emissivity in the regime that quantum effects are important. Chanmugam et al. (1989) compared several approximate equations with numerical results in the cyclotron limit and concluded that Robinson & Melrose (1984) gave the best result. Mahadevan et al. (1996) found approximate formulae for the θ-averaged emission coefficient by fitting to a direct numerical evaluation of the emissivity.

Wardzinski & Zdziarski (2000) combined the approximate equations in Petrosian (1981) and Petrosian & McTiernan (1983) to find an approximate emissivity accurate over a larger range of temperature. Their expressions contain a slight discontinuity, however, because they joined two asymptotic limits without smoothing the intermediate regime. They also found an approximate θ-averaged emissivity.

For polarized light, Kawabata (1964) and Meggitt & Wickramasinghe (1982) gave complicated but exact integral expressions for the specific emissivities in the Stokes formalism, but they did not provide any easily evaluated approximations. Väth & Chanmugam (1995) used the results of Robinson & Melrose (1984) to obtain the approximate equations and compared the results with a direct numerical evaluation of the emissivity in the cyclotron regime.

We began this work because, in attempting to calculate polarized emission spectra for our simulation, we found we needed to evaluate the accuracy of earlier approximate expressions in the regime of interest to us. Here we provide what we hope is a

transparent, well-documented procedure that will enable others to avoid our descent into the minutiae of synchrotron theory. Our MBS calculator has a broad range of validity (described in Section 4) and should therefore be useful for anyone seeking to obtain or test approximate expressions in their domain of interest.

The main approximations we make are (1) $(\nu/\nu_{\rm p})^2 \gg 1$ and (2) $(\nu/\nu_{\rm p})^2(\nu/\nu_{\rm c}) \gg 1$, where the electron plasma frequency

$$\nu_{\rm p} \equiv \left(\frac{n_e e^2}{\pi m_e}\right)^{1/2} = 8980 n_e^{1/2}\,{\rm Hz} \tag{1}$$

(we use Gaussian/cgs units throughout) and the electron cyclotron frequency

$$\nu_{\rm c} \equiv \frac{eB}{2\pi m_e c} = 2.8\times 10^6 B\,{\rm Hz}. \tag{2}$$

When these conditions are violated the index of refraction is noticeably different from 1 and corrections must be made throughout our formalism. We also assume that the magnetic field strength is weak enough such that quantum effects can be neglected (see discussion in Brainerd & Lamb 1987 for details).

The plan of this paper is as follows. In Section 2, we fix notation by writing down the equations of polarized radiative transfer in Stokes and Cartesian polarization bases. In Section 3, we discuss methods for calculating the emission and absorption coefficients for a general distribution function. In Section 4, we recall the usual asymptotic expressions that can be used as code checks. In Section 5, we describe our numerical code, called `harmony`. In Section 6, we evaluate the accuracy of earlier work and provide a convenient fitting formula for the total emissivity (and therefore absorptivity) of thermal electrons with $\Theta_e \equiv kT_e/(m_e c^2) \gtrsim 0.5$. Appendix A briefly describes the distinction between emitted and received power. Appendix B describes an accurate and efficient scheme for evaluating high-order Bessel functions.

2. RADIATIVE TRANSFER

We are concerned with electromagnetic wave propagation at frequency ν in the frame of a magnetized, ionized plasma. The plasma may have a thermal electron component with dimensionless temperature Θ_e; there may also be a nonthermal component in the electron distribution.

In the regime of interest an electromagnetic wave can be written as a sum of the magnetoionic modes of the plasma, the ordinary (O) and extraordinary (X) modes. In the simplest case of a cold plasma, for which the thermal speed is much less than the phase velocities of waves in the plasma, these modes are nearly circularly polarized except for propagation in a narrow range of angles perpendicular to the field. In general the modes are elliptically polarized.

The polarization properties of the magnetoionic modes are described by a pair of orthonormal basis vectors $\mathbf{e}_O$ and $\mathbf{e}_X$, which can be written in terms of unit vectors along the wavevector $\mathbf{k}$, along $\mathbf{k}\times\mathbf{B}$, and perpendicular to both $\mathbf{k}$ and $\mathbf{B}$. Let T_O (T_X) be the ratio of coefficients along the two transverse components of the polarization vector of the ordinary (extraordinary) mode, with $|T_X| \leqslant 1$. In other words, $|T_{O,X}|$ are the axial ratios of the orthogonal polarization ellipses, so that $T_O T_X = -1$. Then

$$\mathbf{e}_O \equiv \{e_{O1}, e_{O2}\} = \frac{1}{\sqrt{T_X^2+1}}\{-1, iT_X\} \tag{3}$$

and

$$\mathbf{e}_X \equiv \{e_{X1}, e_{X2}\} = \frac{1}{\sqrt{T_X^2+1}}\{T_X, i\}, \tag{4}$$

where $\{x, y\}$ are the Cartesian components of a vector in the plane perpendicular to the direction of propagation $\hat{z}$, and $\hat{y}$ is perpendicular to the magnetic field so that $\hat{x}\times\hat{y} \equiv \hat{z}$. The electric field of mode A is $\mathbf{E} = E\mathbf{e}_A \exp(ikz - i\omega t)$. In writing these equations we have assumed that the polarization modes are orthogonal, valid when $\nu^3/({\nu_{\rm p}}^2\nu_{\rm c}) \gg 1$.

2.1. Descriptions of Polarized Radiation

The polarized intensity is most familiarly described by the Stokes vector $I_S = \{I, Q, U, V\}$; here, all components have the usual intensity units, $dE/dtd^2xd\nu d\Omega$, i.e., energy per unit time per unit area per unit frequency per unit solid angle.

The polarized intensity can also be described in terms of a polarization tensor written in a Cartesian coordinate basis (* denotes complex conjugate):

$$I_{ij} \equiv \frac{I}{E^2}\langle E_i E_j^*\rangle = \frac{1}{2}\begin{pmatrix} I+Q & U+iV \\ U-iV & I-Q\end{pmatrix}, \tag{5}$$

where $i, j \in \{x, y\}$ and the prefactor converts the tensor to intensity units.

Finally, the polarized intensity can be described by a polarization tensor in the mode basis

$$\begin{aligned} I_{AB} &= e^*_{Ai} e_{Bj} I_{ij} \\ &= \frac{1}{2}\begin{pmatrix} I - Q\cos\chi - V\sin\chi & -V\cos\chi + Q\sin\chi - iU \\ -V\cos\chi + Q\sin\chi + iU & I + Q\cos\chi + V\sin\chi\end{pmatrix} \end{aligned} \tag{6}$$

where $A, B \in \{O, X\}$ and $\chi = \tan^{-1} T_X$.

2.2. Polarized Radiative Transfer

In the Stokes basis in a uniform plasma the radiative transfer equation is

$$\frac{d}{ds} I_S = J_S - \mathbf{M}_{ST} I_T, \tag{7}$$

where $J_S = \{j_I, j_Q, j_U, j_V\}^{\rm T}$ contains the emission coefficients, which have units of $dE/dtdVd\nu d\Omega$, and the Mueller matrix $\mathbf{M}_{ST}$ is

$$\mathbf{M}_{ST} \equiv \begin{pmatrix} \alpha_I & \alpha_Q & \alpha_U & \alpha_V \\ \alpha_Q & \alpha_I & r_V & -r_U \\ \alpha_U & -r_V & \alpha_I & r_Q \\ \alpha_V & r_U & -r_Q & \alpha_I\end{pmatrix}. \tag{8}$$

The parameters α_i are the absorption coefficients and r_Q, r_U, and r_V are what we will call Faraday mixing coefficients. j_U, α_U, and r_U are zeros for our choice of basis vectors. Below, we will provide a scheme for evaluating the emission and absorption coefficients.

In the Cartesian polarization tensor basis in a uniform plasma the transfer equation is

$$\frac{dI_{ij}}{ds} = J_{ij} - \mu_{ijkl} I_{kl}, \tag{9}$$

where the tensor μ describes absorption and Faraday rotation.

In the mode basis in a uniform plasma

$$\frac{dI_{AB}}{ds} = J_{AB} - \mu_{ABCD} I_{CD}. \tag{10}$$

Contracting the indices, we define α_A by

$$\frac{dI_{AA}}{ds} = -\alpha_A I_{AA}, \tag{11}$$

for radiation consisting of a single mode in the absence of emission and Faraday rotation.

3. MAGNETOBREMSSTRAHLUNG EMISSION AND ABSORPTION

We are now ready to calculate absorption and emission coefficients. These are frame-dependent. We will evaluate them in the plasma center-of-momentum frame (the expressions given below do not assume this). The total emission and absorption coefficients can be transformed using the Lorentz invariance of j_ν/ν^2 and $\nu\alpha_\nu$. The transformation of the full absorption matrix will be discussed in future work.

3.1. Emissivity

A consistent procedure for calculating the emission and absorption coefficients can be found in Melrose & McPhedran (1991). Beginning with their Equation (22.20), rotating the velocity potentials V_i onto a basis where the z-direction is aligned with the wavevector, and introducing appropriate leading constants, the emissivity in the Cartesian polarization basis is

$$J_{ij} = \frac{2\pi e^2\nu^2}{c}\int d^3p\, f \sum_{n=1}^{\infty}\delta(y_n)\, K_{ij} \tag{12}$$

where

$$K_{xx} = M^2 J_n^2(z), \tag{13}$$

$$K_{yy} = N^2 J_n'^2(z), \tag{14}$$

$$K_{xy} = -K_{yx} = -iMNJ_n(z)J_n'(z), \tag{15}$$

and

$$y_n \equiv \frac{n\nu_c}{\gamma} - \nu(1-\beta\cos\xi\cos\theta) = \frac{1}{2\pi}(\omega - n\Omega - k_\parallel v_\parallel) \tag{16}$$

is the argument of the δ function in the resonance condition, $\Omega = 2\pi\nu_c/\gamma$ is the relativistic electron cyclotron angular frequency, $\beta \equiv v/c$, v is the electron speed, ξ is the electron pitch angle,

$$z \equiv \frac{v\gamma\beta\sin\theta\sin\xi}{\nu_c} = \frac{k_\perp v_\perp}{\Omega}, \tag{17}$$

$$M \equiv \frac{\cos\theta - \beta\cos\xi}{\sin\theta}, \tag{18}$$

$$N \equiv \beta\sin\xi, \tag{19}$$

$$f \equiv \frac{dN_e}{d^3x d^3p} = \frac{dn_e}{d^3p} \tag{20}$$

is the electron distribution function, and d^3x and d^3p are differential volumes in real space and momentum space, respectively. Subscripts $\parallel$ and $\perp$ refer to components of vectors parallel and perpendicular to $\mathbf{B}$.

The emissivity in the Stokes basis can be found using the transformation implied by Equation (5):

$$J_S = \frac{2\pi e^2\nu^2}{c}\int d^3p\, f \sum_{n=1}^{\infty}\delta(y_n)K_S \tag{21}$$

where

$$K_I = M^2 J_n^2(z) + N^2 J_n'^2(z), \tag{22}$$

$$K_Q = M^2 J_n^2(z) - N^2 J_n'^2(z), \tag{23}$$

$$K_U = 0, \tag{24}$$

and

$$K_V = -2MNJ_n(z)J_n'(z). \tag{25}$$

In the mode basis

$$J_{AB} = \frac{2\pi e^2\nu^2}{c}\int d^3p\, f \sum_{n=1}^{\infty}\delta(y_n)K_{AB} \tag{26}$$

where

$$K_{XX} = \frac{[MT_X J_n(z) + NJ_n'(z)]^2}{1+T_X^2}, \tag{27}$$

$$K_{OO} = \frac{[MJ_n(z) - NT_X J_n'(z)]^2}{1+T_X^2}, \tag{28}$$

and

$$K_{XO} = K_{OX} = -\frac{[MJ_n(z) - NTJ_n'(z)][MTJ_n(z) + NJ_n'(z)]}{1+T_X^2}. \tag{29}$$

In the cold plasma limit, the axial ratios are (e.g., Melrose 1989)

$$T_{O,X} \equiv T_\pm \approx \frac{2\nu\cos\theta}{\nu_c\sin^2\theta \mp \sqrt{\nu_c{}^2\sin^4\theta + 4\nu^2\cos^2\theta}} \quad \text{for } \nu \gg \nu_p. \tag{30}$$

The polarized emissivities are related to the total emissivity by

$$j_\nu \equiv J_I = J_{xx} + J_{yy} = J_{OO} + J_{XX} \equiv \int d^3p f \eta_\nu, \tag{31}$$

where

$$\eta_\nu \equiv \frac{dE}{d\nu dt d\Omega} \tag{32}$$

is the single-electron emissivity.

3.2. Absorption Coefficients

If the distribution function is thermal then the absorption coefficients follow from Kirchhoff's law. For a nonthermal plasma we must calculate the absorption coefficients directly.

If the plasma is weakly anisotropic (i.e., the anisotropic effect is perturbative) then it is possible to simply relate the absorption coefficients to the anisotropic, antihermitian part of the dielectric tensor. Starting with the dielectric tensor of a magnetized plasma (Equation (22.47) of Melrose & McPhedran 1991, corrected by a factor of $4\pi/\omega^2$, or Equations (10)–(48) of Stix 1992), and using the Plemelj relation to find the imaginary part of the

integral over momentum space (and thus the antihermitian part of the dielectric tensor), we find

$$\mu_{ijkl} = \frac{ce^2}{\nu}\int d^3p\, Df \sum_{n=1}^{\infty}\delta(y_n)K_{ijkl}, \tag{33}$$

where

$$K_{xxxx} = M^2 J_n^2(z), \tag{34}$$

$$K_{xxyx} = K_{xyxx} = K_{xyyy} = K_{yyyx} = -\frac{i}{2}MNJ_n(z)J_n'(z), \tag{35}$$

$$K_{xxxy} = K_{yxxx} = K_{yxyy} = K_{yyxy} = \frac{i}{2}MNJ_n(z)J_n'(z), \tag{36}$$

$$K_{xyxy} = K_{yxyx} = \frac{1}{2}\left[M^2 J_n^2(z) + N^2 J_n'^2(z)\right], \tag{37}$$

$$K_{yyyy} = N^2 J_n'^2(z), \tag{38}$$

all other components of K vanish, and the operator D is

$$Df \equiv \left(\frac{\omega - k_\parallel v_\parallel}{v_\perp}\frac{\partial}{\partial p_\perp} + k_\parallel \frac{\partial}{\partial p_\parallel}\right) f. \tag{39}$$

In writing this equation, we assume that the energy of the absorbed photon is small compared to the width of the distribution function, permitting us to replace a difference with the derivative operator D. For a thermal distribution this requires that $h\nu/kT_e \ll 1$.

In terms of $p = |\mathbf{p}|$ and $\cos\xi$, the operator D is

$$Df = \frac{2\pi\nu}{c\beta}\left(\frac{\partial}{\partial p} + \frac{\beta\cos\theta - \cos\xi}{p}\frac{\partial}{\partial\cos\xi}\right) f, \tag{40}$$

and in terms of γ and $\cos\xi$,

$$Df = 2\pi\nu\left(\frac{1}{m_e c^2}\frac{\partial}{\partial\gamma} + \frac{\beta\cos\theta - \cos\xi}{p\beta c}\frac{\partial}{\partial\cos\xi}\right) f. \tag{41}$$

In the Stokes basis,

$$\alpha_S = -\frac{ce^2}{2\nu}\int d^3p \sum_{n=1}^{\infty}\delta(y_n)Df\, K_S, \tag{42}$$

where subscript S is one of I, Q, U, and V. In the mode basis

$$\alpha_A = -\frac{ce^2}{\nu}\int d^3p \sum_{n=1}^{\infty}\delta(y_n)Df\, K_{AA}, \tag{43}$$

where subscript A is O or X.

Let us explicitly verify Kirchhoff's law for a thermal distribution function in the Stokes basis:

$$J_S - \alpha_S B_\nu = 0, \tag{44}$$

where $B_\nu = (2h\nu^3/c^2)[\exp(h\nu/kT_e) - 1]^{-1}$ is the Planck function. Using Equations (21) and (42), and gathering like terms, this becomes

$$\int d^3p \sum_{n=1}^{\infty}\delta(y_n)K_S\left(\frac{2\pi e^2\nu^2}{c}f + \frac{ce^2}{2\nu}Df\ \ B_\nu\right) = 0. \tag{45}$$

If we make γ the nontrivial momentum space coordinate, then $f = N\exp(-\gamma/\Theta_e)$, where $N(\Theta_e)$ is a normalization constant, and $Df = -2\pi N\nu\exp(-\gamma/\Theta_e)/(m_e c^2\Theta_e)$. This leaves

$$\int d^3p \sum_{n=1}^{\infty}\delta(y_n)K_S\left(\frac{2\pi e^2\nu^2}{c}\right)Ne^{-\gamma/\Theta_e} \times\left(1 - \frac{h\nu/(kT_e)}{\exp(h\nu/(kT_e)) - 1}\right) = O\left(\frac{h\nu}{kT_e}\right). \tag{46}$$

This is consistent with the assumption that the energy of the absorbed photon is small compared to the width of the distribution function; to lowest order in $h\nu/kT_e$ Kirchhoff's law is satisfied.

3.3. Electron Distribution Function

The electron distribution can be written using a variety of momentum space coordinates, and this can be a source of some confusion. For example, with respect to the auxiliary momentum coordinates γ, ξ, and ϕ (the longitudinal coordinate), d^3p can be expressed as $m_e^3c^3\gamma^2\beta d\gamma d(\cos\xi)d\phi$ and the distribution function as

$$f \equiv \frac{dn_e}{d^3p} = \frac{1}{m_e^3c^3\gamma^2\beta}\frac{dn_e}{d\gamma d(\cos\xi)\,d\phi} = \frac{1}{2\pi m_e^3c^3\gamma^2\beta}\frac{dn_e}{d\gamma d(\cos\xi)}, \tag{47}$$

where the final equality arises from assuming that the distribution is independent of ϕ. Equation (42) becomes

$$\alpha_S = -\frac{ce^2}{2\nu}\int d\gamma d(\cos\xi)\sum_{n=1}^{\infty}\delta(y_n)\gamma^2\beta D \times\left[\frac{1}{\gamma^2\beta}\frac{dn_e}{d\gamma d(\cos\xi)}\right]K_S \tag{48}$$

and similarly for the absorption coefficients in the mode basis.

The thermal (relativistic Maxwellian) distribution function is

$$\frac{dn_e}{d\gamma d\Omega_p} \equiv \frac{dn_e}{d\gamma d\phi d(\cos\xi)} = \frac{n_e}{4\pi\Theta_e}\frac{\gamma(\gamma^2-1)^{1/2}}{K_2(1/\Theta_e)}\exp\left(-\frac{\gamma}{\Theta_e}\right); \tag{49}$$

$d\Omega_p$ is a differential solid angle in momentum space and K_2 is a modified Bessel function of the second kind.

A useful nonthermal distribution function is the isotropic power-law distribution

$$\frac{dn_e}{d\gamma d\Omega_p} = \frac{n_e^{\rm NT}(p-1)}{4\pi\left(\gamma_{\rm min}^{1-p} - \gamma_{\rm max}^{1-p}\right)}\gamma^{-p} \quad \text{for } \gamma_{\rm min} \leqslant \gamma \leqslant \gamma_{\rm max}, \tag{50}$$

where $n_e^{\rm NT}$ is the number density of nonthermal electrons.

4. ULTRARELATIVISTIC LIMIT

For clarity it is helpful to record the emission and absorption coefficients for a thermal electron distribution and for a power-law distribution of electrons in the ultrarelativistic limit. These are well known but presented here in a consistent set of units and notation so that we can check our numerical results.

The emissivity of a single ultrarelativistic electron can be reduced through a standard approximation (e.g., Westfold 1959;

Ginzburg 1970)

$$\int d\Omega_p \eta_\nu \simeq \frac{\sqrt{3} e^3 B \sin\theta}{m_e c^2} F\left(\frac{\nu}{\nu_{\rm cr}}\right), \tag{51}$$

where $\nu_{\rm cr} = (3/2)\nu_{\rm c} \sin\theta \gamma^2$, and the synchrotron function

$$F(x) \equiv x \int_x^\infty dt\, K_{5/3}(t). \tag{52}$$

The asymptotic expansions of $F(x)$ are

$$F(x) = \left\{ \begin{array}{ll} 2^{2/3}\Gamma(2/3) x^{1/3} + O(x) & \text{for } x \ll 1 \\ \left(\frac{\pi x}{2}\right)^{1/2} \exp(-x)(1 + O(x^{-1})) & \text{for } x \gg 1 \end{array} \right\}. \tag{53}$$

For a thermal distribution with $\Theta_e \gg 1$, $K_2(1/\Theta_e) \simeq 2\Theta_e^2$ and

$$\frac{dn_e}{d\gamma d\Omega_p} \simeq \frac{n_e \gamma^2}{8\pi\Theta_e^3} \exp(-\gamma/\Theta_e). \tag{54}$$

For $\nu \ll \nu_{\rm s} \equiv (2/9)\nu_{\rm c}\Theta_e^2 \sin\theta$, the small-$x$ limit of Equation (53) can be used, most of the emission comes from electrons with $\gamma \sim \Theta_e$, and the emissivity is

$$j_\nu \simeq \frac{2^{4/3}\pi}{3} \frac{n_e e^2 \nu_{\rm s}}{c\Theta_e^2} X^{1/3}, \tag{55}$$

where

$$X \equiv \frac{\nu}{\nu_{\rm s}}. \tag{56}$$

For $\nu \gg \nu_{\rm s}$ the large-x limit of Equation (53) applies. The integrand is proportional to $\exp(-\gamma/\Theta_e - \nu/\nu_{\rm cr})$, where $\nu_{\rm cr} \sim \gamma^2$, so the peak emission is from electrons with $\gamma \sim (\nu\Theta_e/(\nu_{\rm c}\sin\theta))^{1/3}$. Then,

$$j_\nu \simeq n_e \frac{\sqrt{2}\pi e^2 \nu_{\rm s}}{6\Theta_e^2 c} X \exp(-X^{1/3}), \tag{57}$$

and the integral has been evaluated using the method of steepest descent (Petrosian 1981).

For the isotropic power-law distribution of electrons the integration can be done explicitly without using the asymptotic expansion for $F(x)$ if $p > 1$. Most of the emission comes from electrons with $\gamma^2 \sim \nu/\nu_{\rm c}$, and the emissivity is (Blumenthal & Gould 1970)

$$j_\nu = n_e^{\rm NT} \left(\frac{e^2\nu_{\rm c}}{c}\right) \frac{3^{p/2}(p-1)\sin\theta}{2(p+1)\left(\gamma_{\rm min}^{1-p} - \gamma_{\rm max}^{1-p}\right)} \Gamma\left(\frac{3p-1}{12}\right) \times \Gamma\left(\frac{3p+19}{12}\right) \left(\frac{\nu}{\nu_{\rm c}\sin\theta}\right)^{-(p-1)/2} \tag{58}$$

for $\gamma_{\rm min}^2 \ll \nu/\nu_c \ll \gamma_{\rm max}^2$. The absorptivity, famously, cannot be obtained from Kirchhoff's law, but can be evaluated using Equation (42). The result is (see, e.g., Rybicki & Lightman 1979 for a discussion)

$$\alpha_\nu = n_e^{\rm NT} \left(\frac{e^2}{\nu m_e c}\right) \frac{3^{(p+1)/2}(p-1)}{4\left(\gamma_{\rm min}^{1-p} - \gamma_{\rm max}^{1-p}\right)} \Gamma\left(\frac{3p+2}{12}\right) \times \Gamma\left(\frac{3p+22}{12}\right) \left(\frac{\nu}{\nu_{\rm c}\sin\theta}\right)^{-(p+2)/2}, \tag{59}$$

again for $\gamma_{\rm min}^2 \ll \nu/\nu_c \ll \gamma_{\rm max}^2$. Note that this expression for the absorptivity is proportional to $n_e^{\rm NT} e^2/(\nu m_e c)$. Since $(n_e^{\rm NT} e^2/m_e)^{1/2}$ is a plasma frequency for the nonthermal electrons, the absorption coefficient has the expected dimensions of 1/length.

5. NUMERICAL CALCULATIONS

The emission and absorption coefficients all require the numerical evaluation of expressions of the following form:

$$\int_1^\infty d\gamma \int_{-1}^1 d\cos\xi \sum_{n=1}^\infty \delta(y_n) I(n, \xi, \gamma), \tag{60}$$

where I is some function, ξ is the electron pitch angle, γ is the electron Lorentz factor, and n is the harmonic index (see, e.g., Equation (21)), and the resonance condition is

$$y_n \equiv \frac{n\nu_{\rm c}}{\gamma} - \nu(1 - \beta\cos\xi\cos\theta) = 0, \tag{61}$$

which involves all three independent variables: γ, ξ, and n. Recall that the resonance condition arises because each electron emits only at integer multiples of its own cyclotron frequency, Doppler shifted to the plasma rest frame.

5.1. Previous Work

Many have evaluated the absorption and emission coefficients numerically. Early efforts include the calculation of $j_\nu(\theta)$ by Takahara & Tsuruta (1982) for n up to several hundred. Melia (1994) calculated the emissivity numerically for $\theta = \pi/2$.

The emissivity is sharply peaked at particular ν; the integrand is not well behaved. Mahadevan et al. (1996) resolved the resulting numerical difficulty by replacing the δ function with a broadening function of adjustable frequency width and evaluating the full three-dimensional integral. Only an observer angle-averaged emission coefficient, $\bar{j}_\nu \equiv \int_0^1 j_\nu(\theta) d(\cos\theta)$, was found. The resonance condition was also used to simplify the integral.

Marcowith & Malzac (2003) found the angle-averaged emission coefficient by two methods. The first was similar to Mahadevan et al. (1996) except that a different broadening function was used. Another method, "direct integration," used the resonance condition to select an observer angle.

Wolfe & Melia (2006) calculated the angle-averaged single-particle emissivity and extended the summation to the 990th harmonic to increase the accuracy of the result. The calculation was done by replacing the δ function with a broadening function, as in Mahadevan et al. (1996). The single-particle emissivity was then fitted with >1500 coefficients over the range $-1 < \log_{10}(\nu/\nu_{\rm c}) < 2$ and $0.1 < \beta < 0.98$. For the thermal emissivity, they explicitly evaluated the γ integral for $\beta < 0.97$; for $\beta > 0.97$ they used an approximation from Petrosian (1981). They restricted their calculation to $-1 < \log_{10}(\nu/\nu_{\rm c}) < 2$; they did not offer an explicit control for the accuracy of the $n \leqslant 990$ approximation for a particular γ.

5.2. Numerical Procedure

We use the resonance condition (61) to eliminate $\cos\xi$ from Equation (60). This is simpler than eliminating γ (because the resonance condition is quadratic in β), and also simpler than

eliminating n (because n must take on integer values). The remaining integral has the form

$$\int_{\gamma_-}^{\gamma_+} d\gamma \sum_{n=n_-}^{\infty} \left(\frac{1}{\nu\beta|\cos\theta|} \right) I(n, \xi, \gamma) \tag{62}$$

and the term in parentheses, $|dy_n/d\cos\xi|^{-1}$, comes from integrating over the δ function. The range of integration is now restricted by the requirements that $|\cos\xi| < 1$ and that γ be real.

The limits on the γ integration follow from $|\cos\xi| < 1$. Write the resonance condition

$$\cos\xi = \frac{\gamma\nu - n\nu_c}{\gamma\nu\beta\cos\theta}, \tag{63}$$

and set $\cos\xi = \pm 1$ to find

$$\gamma_\pm = \frac{n\nu_c/\nu \pm |\cos\theta|\sqrt{(n\nu_c/\nu)^2 - \sin^2\theta}}{\sin^2\theta}. \tag{64}$$

Note that γ_- reaches a minimum of 1 for $n\nu_c/\nu = 1$, so $\gamma_- \geqslant 1$.

The argument of the square root in Equation (64) must be non-negative. This restricts the range of n to

$$n \geqslant n_- = \frac{\nu}{\nu_c}|\sin\theta|. \tag{65}$$

At n_-, $\gamma_+ = \gamma_-$.

We need to choose an order to evaluate the integrals (sums) in Equation (62). If the sum is done first then the remaining integrand is a rapidly varying, comb-like, function of γ for θ close to $\pi/2$. If the γ integration is done first the remaining summand is a smooth function of n and therefore more numerically tractable. We therefore do the γ integration first.

5.3. Upper Limit of Summation

The summation in Equation (62) extends to $n = \infty$, so for numerical summation we must either map n onto a finite domain or else choose an upper limit n_+ to the sum, beyond which the integrand is negligible. We have taken the latter approach.

For the special case of a thermal electron distribution we set $n_+ = Cn_{\rm peak}$, where the integrand peaks near $n_{\rm peak}$ and $C > 1$ is a dimensionless constant. At $\nu \ll \nu_c\Theta_e^2$, the integrand peaks when $J_n(z)$ peaks, at $z/n \simeq 1$, i.e., near

$$n = n_{\rm peak} = \gamma\frac{\nu}{\nu_c}(1 - \beta^2\cos^2\theta). \tag{66}$$

The thermal distribution is proportional to $\exp(-\gamma/\Theta_e)/K_2(1/\Theta_e)$. This peaks at $\gamma \sim 1 + \Theta_e$ for all Θ_e, so

$$n_{\rm peak} \simeq (\Theta_e + 1)(\nu/\nu_c)(1 - \beta^2\cos^2\theta) \tag{67}$$

is a good estimate for all Θ_e.

For $\nu \gg \nu_c\Theta_e^2$ we can use the asymptotic expression for the single electron emissivity to estimate $n_{\rm peak}$ (see Section 5). The peak is near the peak of the function $\exp[-\gamma/\Theta_e - \nu/(\gamma^2\nu_c)]$, so most of the emission comes from electrons with $\gamma = (2\Theta_e\nu/\nu_c)^{1/3}$.

Combining the low-frequency and high-frequency estimates for $n_{\rm peak}$,

$$n_+ = C\left[\Theta_e + 1 + \left(2\Theta_e\frac{\nu}{\nu_c}\right)^{1/3}\right]\frac{\nu}{\nu_c}(1 - \beta^2\cos^2\theta). \tag{68}$$

Typically $C = 10$ gives adequate accuracy.

For a nonthermal distribution we take an adaptive approach. We sum over successive intervals $[n_-, n_- + \Delta n]$, $[n_- + \Delta n + 1, 2(n_- + \Delta n)]$, $[2(n_- + \Delta n) + 1, 4(n_- + \Delta n)]$, etc., until the fractional contribution from the last interval is smaller than a preset tolerance. This procedure yields fast convergence except for exotic electron distribution functions. Some knowledge of the distribution is required, however, to set Δn.

5.4. Numerical Considerations

Accurate, efficient evaluation of the Bessel function $J_n(z)$ for $n \gg 1$ is essential for our calculation. When n is small, any mathematical library gives an accurate, efficient result. As n increases, however, standard mathematical libraries slow down, become inaccurate, and fail. In our calculations, the argument z and order n of the Bessel functions can be large and are typically comparable in size (one can show that $z/n < 1$). Standard asymptotic expansions (see Abramowitz & Stegun 1970) are unsatisfactory because they typically assume $z \gg n$ or vice versa. We calculate J_n using a special-purpose code based on asymptotic expansions discussed in Chishtie et al. (2005), who divide the arguments into three regimes and provide asymptotic expansions for each regime. Details of our scheme are discussed in Appendix B.

The summation over n is done as an explicit sum at small n and as an integral at large n. The same approach was used by Takahara & Tsuruta (1982). Approximating the sum as an integral at large n increases both speed and, in many cases, accuracy. The breakpoint, n_I, between summation and integration is set heuristically. Typically, we use $n_I = 30$ for the parameters of interest to us.

We integrate using the GNU Scientific Library's QAG integrator, which is fast, robust, and publicly available. One subtlety here is connected to the narrow extent of the γ integrand when ν is large (this narrow extent permits one to use the method of steepest descent in evaluating Equation (57)). If the domain of integration is not set correctly then the integrator can fail to resolve the peak and the emissivity, for example, will be underestimated.

Finally, note that Equation (62) fails for $\theta = \pi/2$ because the δ function does not contain $\cos\xi$ and so cannot be used to eliminate the $\cos\xi$ integral. But since $j_\nu(\theta)$ is a smooth function of θ with a maximum at $\theta = \pi/2$, we simply avoid evaluating the emissivity at $\theta = \pi/2$ by extrapolating from nearby θ. The error is of the same order as a single integration because of the zero slope around the peak. The only penalty is that the time needed to find j_ν is doubled compared to the calculation at other θ.

6. VERIFICATION OF CALCULATION

6.1. Monoenergetic Electrons

The angle-averaged synchrotron emissivity of ultrarelativistic monoenergetic electrons is

$$\bar{j}_\nu(\nu, \gamma) \simeq n_e\frac{1}{2}\int_{-1}^{1}\frac{\sqrt{3}e^3B\sin\theta}{4\pi m_ec^2}F\left(\frac{\nu}{\nu_{\rm cr}}\right)d(\cos\theta) \equiv n_e\bar{\eta}_\nu. \tag{69}$$

The single-particle emissivity can be approximated as (Crusius & Schlickeiser 1986, 1988; Schlickeiser & Lerche 2007)

$$\bar{\eta}_\nu(\nu, \gamma) \approx \frac{\pi e^2\nu}{2\sqrt{3}c\gamma^2}{\rm CS}\left[\frac{2\nu}{3\nu_c\gamma^2}\right], \tag{70}$$

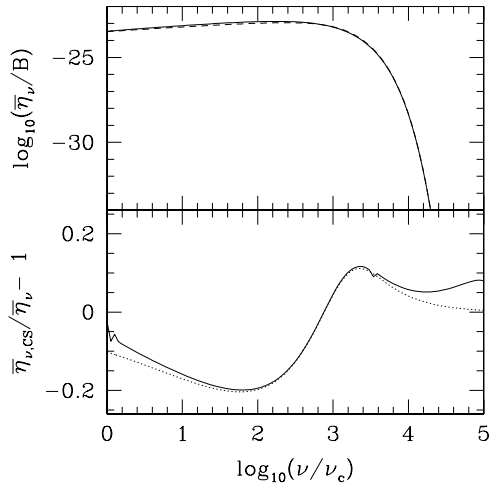

Figure 1. Upper panel: the angle-averaged single-particle emissivity $\bar{\eta}_\nu/B$, in cgs units, at $\beta = 0.999$. The solid line is the result of `harmony`, and the dashed line is calculated by using the approximate Equation (70). Lower panel: the solid line is the relative difference of Equation (70) and the result of `harmony`, and the dotted line is the difference between Equation (70) and the ultrarelativistic limit Equation (69).

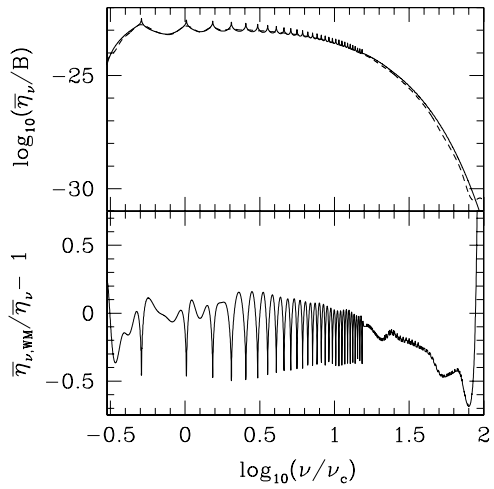

Figure 2. Upper panel: the angle-averaged single-particle emissivity $\bar{\eta}_\nu/B$, in cgs units, at $\beta = 0.86$. The solid line is result of `harmony`, and the dashed line is result of Wolfe & Melia (2006) multiplied by a factor of π^2 (which we cannot explain). Lower panel: the relative difference of $\bar{\eta}_\nu$. The difference compared to Wolfe & Melia (2006, their Figure 3) seems to be due to better resolution of the cyclotron peaks in our calculation.

where the function $\mathrm{CS}(x)$ is given by

$$\mathrm{CS}(x) = \frac{x^{-2/3}}{0.869 + x^{1/3}\exp(x)}. \quad (71)$$

We compute an approximation to the emissivity of a monoenergetic distribution by using a narrow Gaussian in energy; for small enough energy width ΔE the emissivity is independent of ΔE. Figure 1 compares Equation (70) with the `harmony` result and the ultrarelativistic limit Equation (69). At high frequency, `harmony` underestimates the emissivity because the integrand becomes too narrow to be resolved numerically. Evidently, Equation (71) has a maximum error of order ≈20%.

Wolfe & Melia (2006) fit the angle-averaged single-particle emissivity and provide a code that reproduces their fitting function. Figure 2 compares results of `harmony` with their code, with the same parameters as their Figure 3(c). The relative error of their fitting formula, compared with our "exact" numerical calculation, is somewhat larger than the error shown in their Figure 3(c), perhaps due to our better resolution of the cyclotron peaks.

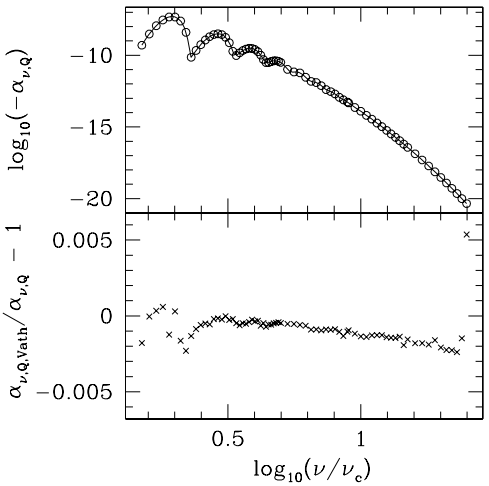

Figure 3. Upper panel: the absorption coefficients α_Q in cm^{-1} at $kT_e = 10.0\,\mathrm{keV}$, $\theta = 60°$. The solid lines are from `harmony`, whereas the circles are data from Table 4 in Väth & Chanmugam (1995). Lower panel: relative difference of the data from Väth & Chanmugam (1995) and `harmony`. There is a trend of deviation from zero as ν increases. The trend is removed if `harmony` is run at $kT_e = 9.998\,\mathrm{keV}$. Similar trends are also seen in the plots of other absorption coefficients in Väth & Chanmugam (1995). The maximum relative difference is 0.2% if the last two data points are dropped.

6.2. Thermal Distribution

At large ν and Θ_e, our emissivity agrees with the ultrarelativistic limit; this is discussed in greater detail in Section 7.

At low ν and Θ_e, where cyclotron features are prominent, we have compared our results with those in Väth & Chanmugam (1995) and Chanmugam et al. (1989) and found good agreement. Note that although the expressions presented in Chanmugam et al. (1989) and Väth & Chanmugam (1995) allow for refractive index ≠ 1, the deviation of the refractive index from 1 is small in our test examples, so we expect good agreement.

First, we calculate the absorption coefficients in the Stokes basis and compare with Väth & Chanmugam (1995). Figure 3 shows that α_Q calculated with `harmony` is within 0.2% of the results of Väth & Chanmugam (1995). α_I and α_V have similar relative differences. We then calculate the absorption coefficients in the mode basis. Figure 4 compares α_O from Chanmugam et al. (1989) with the results of `harmony`. Using the cold plasma approximation of T_X (Equation (30)) in `harmony`, the relative differences of $\alpha_{O,X}$ are $\leqslant$0.2% compared with the results of Chanmugam et al. (1989).

As another check, at $\theta = \pi/2$, we eliminate the γ integration using the δ function. Since at $\theta = \pi/2$ the β dependence of the resonance condition is eliminated, we are left with a single value for γ and a two-dimensional integral in $\cos\xi$ and n. This integration gives the same result as the γ–n integration.

6.3. Angle-averaged Thermal Emission

Mahadevan et al. (1996) provide a fitting formula to calculate the observer angle-averaged emissivity $\bar{j}_\nu$ for a thermal distribution. Coefficients of the fitting formula are given for seven temperatures between 7×10^8 K and 3.2×10^{10} K, and the fractional errors are given for each temperature. Figure 5 compares our calculation with the fitting formula at 3.2×10^{10} K. We find

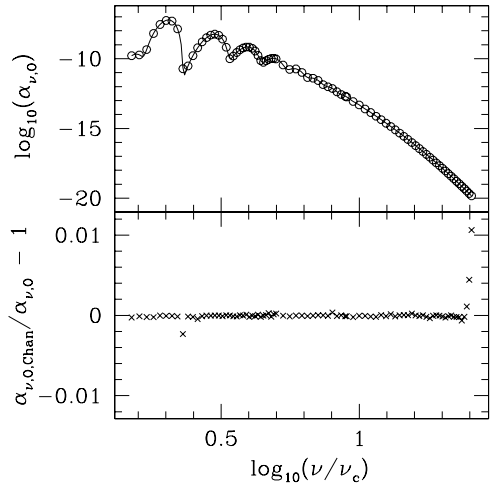

Figure 4. Upper panel: the absorption coefficients α_O in cm^{-1} at $kT_e = 10.0\,\mathrm{keV}$, and $\theta = 60^\circ$. The solid lines are from `harmony` with cold plasma T_X in Equation (30), and the circles are data from Table 6B in Chanmugam et al. (1989). Lower panel: the crosses are relative differences of the data from Chanmugam et al. (1989) and `harmony` with cold plasma T_X.

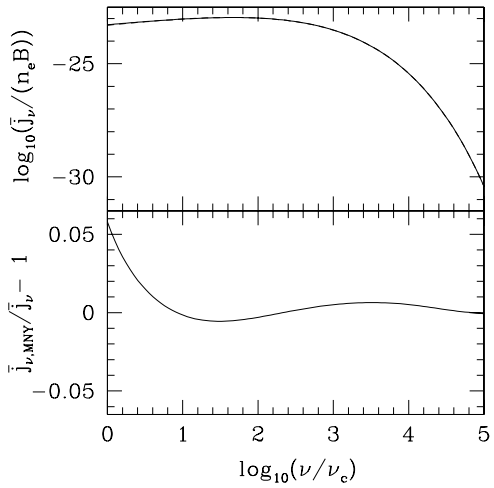

Figure 5. Upper panel: the angle-averaged thermal emissivity $\bar{j}_\nu/(n_e B)$ in cgs units, at $T = 3.2 \times 10^{10}\,\mathrm{K}$, for `harmony` (solid line) and fitting formula in Mahadevan et al. (1996) (dashed line). Lower panel: the relative difference of $\bar{j}_\nu$.

good agreement with their formula and reproduce their maximum error.

6.4. Nonthermal Electron Distribution

For a power-law distribution in the ultrarelativistic limit our absorption and emission coefficients agree with Equations (58) and (59). Figures 6 and 7 show the emission and absorption coefficients for $p = 3$, $\gamma_{\min} = 1$, $\gamma_{\max} = 1000$, and $\theta = 60^\circ$. For $\gamma_{\min}^2 \ll \nu/\nu_c \ll \gamma_{\max}^2$ the relative errors in Equations (58) and (59) approach 10^{-3}, while the errors diverge for smaller and larger ν/ν_c.

Our code can also handle an electron distribution with pitch-angle dependence. One example is the anisotropic nonthermal emission calculated in Fleishman & Melnikov (2003). We reproduce their Figure 1 in our Figure 8. We do not have the Fleishman & Melnikov data, so we cannot make a quantitative comparison, but a comparison by eye suggests that our results reproduce theirs quite well.

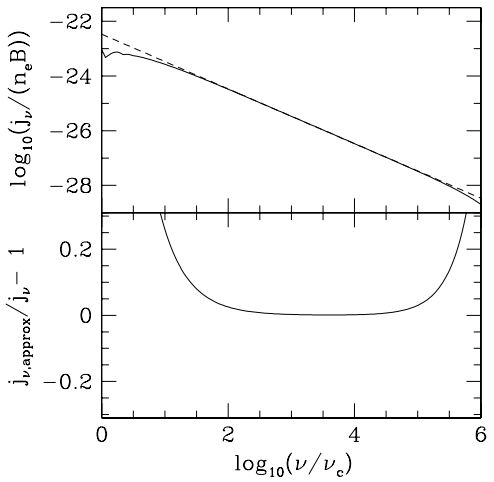

Figure 6. Upper panel: the emissivity $j_\nu/(n_e B)$, in cgs units, for $p = 3$, $\gamma_{\min} = 1$, $\gamma_{\max} = 1000$, and $\theta = 60^\circ$. The solid line is the result of `harmony`, and the dashed line is calculated by using Equation (58). Lower panel: the relative difference of j_ν. The error is smallest for $\gamma_{\min}^2 \ll \nu/\nu_c \ll \gamma_{\max}^2$. At smaller and larger frequencies, the error diverges.

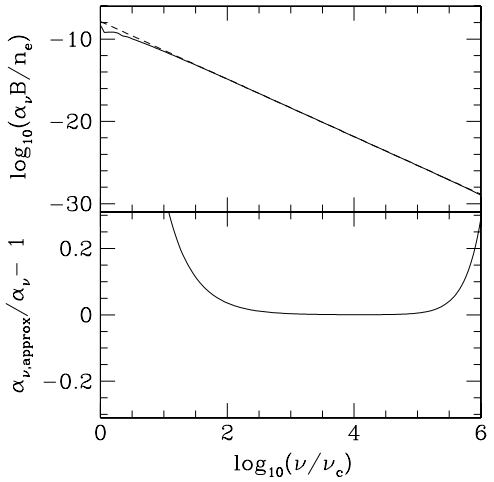

Figure 7. Upper panel: the absorption coefficient $\alpha_\nu B/n_e$, in cgs units, for $p = 3$, $\gamma_{\min} = 1$, $\gamma_{\max} = 1000$, and $\theta = 60^\circ$. The solid line is the result of `harmony`, and the dashed line is calculated by using Equation (59). Lower panel: the relative difference of j_ν. The error is smallest for $\gamma_{\min}^2 \ll \nu/\nu_c \ll \gamma_{\max}^2$. At smaller and larger frequencies, the error diverges.

7. APPROXIMATE EQUATION

Motivated by the above discussion, and by the ultrarelativistic limit discussed above, we introduce the following approximate expression for the thermal MBS emissivity:

$$j_\nu = n_e \frac{\sqrt{2}\pi e^2 \nu_s}{3K_2(1/\Theta_e)c}(X^{1/2} + 2^{11/12}X^{1/6})^2 \exp(-X^{1/3}). \quad (72)$$

Equation (72) combines Equation (26) of Petrosian (1981) and Equation (55). All three equations are shown in Figure 9, which shows that Equation (72) is accurate over a much larger range of frequency.

Figures 10 and 11 are contour plots of the accuracy of Equation (72) over a wide range of Θ_e and frequencies for $\theta = 30^\circ$ and $\theta = 80^\circ$, respectively. These plots verify that our scheme accurately reproduces the high-frequency limit given by Equation (57), which coincides with Equation (72). As a crude guide to the regime of validity of Equation (72), we estimate that the error becomes of order unity for $\Theta_e \simeq (\nu/(\nu_c \sin\theta))^{-1/5}$.

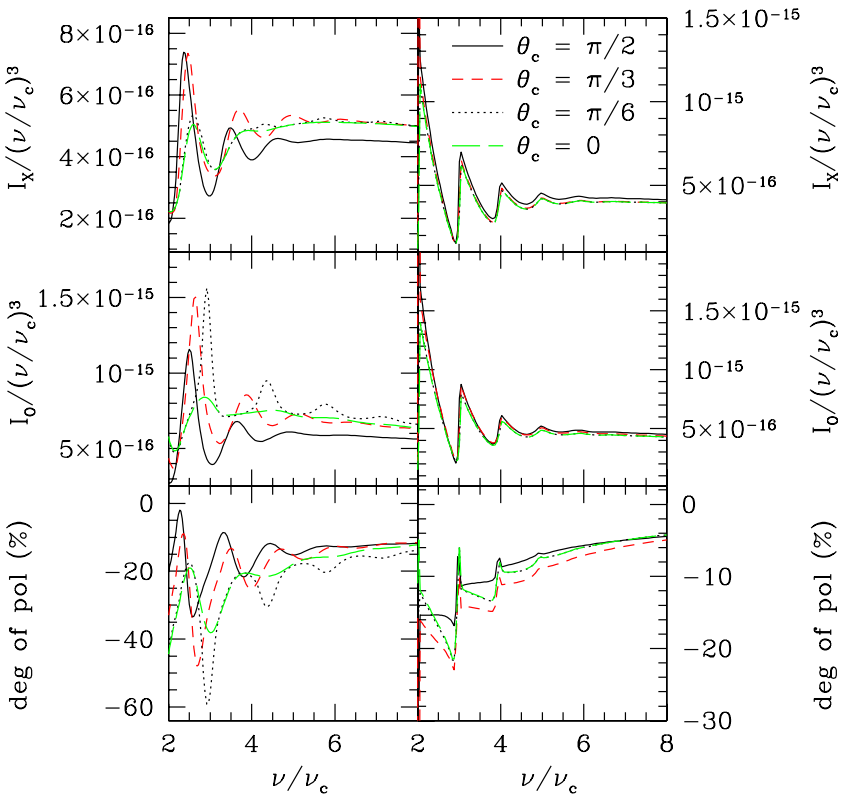

Figure 8. Reproduction of Figure 1 in Fleishman & Melnikov (2003). $I_X/(\nu/\nu_c)^3$, $I_O(\nu/\nu_c)^3$, and degree of polarization are plotted as functions of frequency. Intensity I_A is defined as j_A/α_A, where A is O (ordinary mode) or X (extraordinary mode). Degree of polarization is defined as $(I_X - I_O)/(I_X + I_O)$. The panels on the left (right) are calculated with assumption that $\cos\theta = 0.8(0.2)$. In both cases, $\nu_p/\nu_c = 0.4$ and the exponent of the momentum power-law distribution is 5. Cold plasma approximation of T_X is used in the calculation using `harmony`.

(A color version of this figure is available in the online journal.)

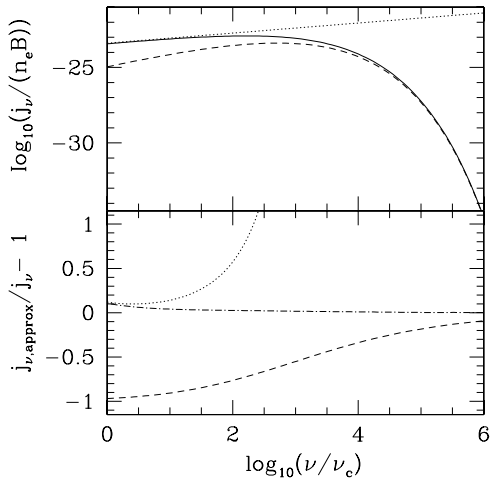

Figure 9. Upper panel: the emissivity $j_\nu/(n_e B)$, in cgs units, for $\Theta_e = 10$, $\theta = 60^\circ$. The solid line is the result of `harmony`. The dashed line shows Equation (26) of Petrosian (1981), and the dotted line shows Equation (55). The dot-dashed line (which overlaps the solid line) shows the combined Equation (72). Lower panel: the relative difference of the approximate equations.

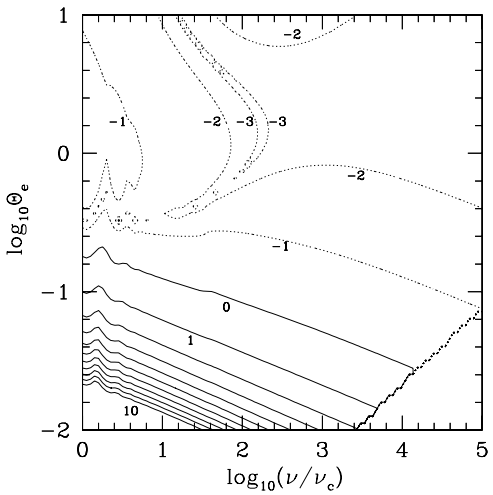

Figure 10. Logarithm of the relative error of the approximated equation (72) of emissivity j_ν, at $\theta = 30^\circ$. The dotted lines are contours of negative integers, and the solid lines are zero and positive integers up to 10. The lower right corner is ignored since the emissivity is too low (cutoff $= 1 \times 10^{-250}$ [cgs]).

8. SUMMARY

We have described and verified an accurate, efficient scheme for evaluating MBS emission and absorption coefficients for polarized emission for an arbitrary electron distribution function. The relationship between the coefficients in the Stokes, Cartesian polarization, and mode polarization bases is given in Section 2.

For each coefficient we must evaluate a two-dimensional integral of the form in Equation (62). We use a publicly available numerical integration method. The integrand depends on Bessel functions of the first kind of high-order n, so along the way we have developed an efficient method for evaluating high-order Bessel functions. This method is described in Appendix B.

We have used the numerical results to evaluate the accuracy of several approximate analytic expressions that appear in the

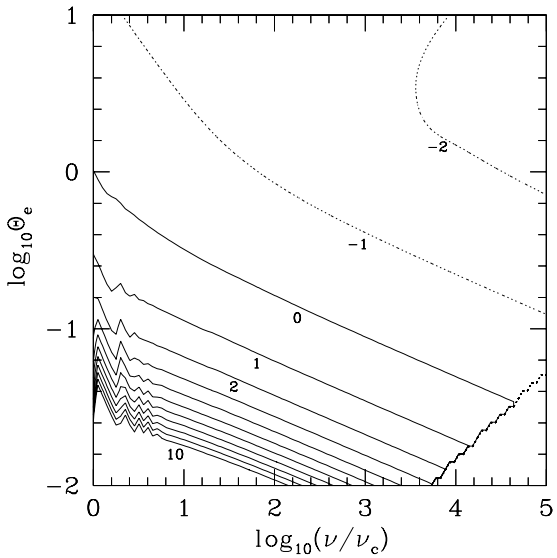

Figure 11. Logarithm of the relative error of the approximated equation (72) of emissivity j_ν, at $\theta = 80°$. The dotted lines are contours of negative integers, and the solid lines are zero and positive integers up to 10. The lower-right corner is ignored since the emissivity is too low (cutoff $= 1 \times 10^{-250}$ [cgs]).

literature, and we have also verified earlier numerical work (e.g., Petrosian 1981; Robinson & Melrose 1984; Mahadevan et al. 1996).

Our code, called `harmony`, is available at http://rainman.astro.illinois.edu/codelib/.

This work was supported by the National Science Foundation under grants AST 00-93091, PHY 02-05155, and AST 07-09246, and by a Richard and Margaret Romano Professorial Scholarship, a Sony faculty fellowship, and a University Scholar appointment to C.F.G. Portions of this work were performed while C.F.G. was a member at the Institute for Advanced Study during academic year 2006–2007.

APPENDIX A

ADDITIONAL DOPPLER FACTOR IN EMISSIVITY

There is some confusion in the literature about the expression for the single-electron emissivity, which can be calculated directly from Maxwell's equations (see Bekefi 1966). This confusion is connected to discussions of the distinction between received and emitted power first noted by Ginzburg & Syrovatskii (1968) and by Pacholczyk (1970), and discussed by Scheuer (1968), Rybicki & Lightman (1979, Section 6.7), and very clearly by Blumenthal & Gould (1970, Sections 4.3 and 4.4). So, for example, Wardzinski & Zdziarski (2000, Section 2.1) state that an additional Doppler factor $(1 - \beta\mu\cos\theta)^{-1}$ should have appeared in their expression for the single-electron emissivity η_ν (see their Equation (1)), but that this factor "disappears in the case of an electron moving chaotically." Here we show that there is no such factor.

To find the emissivity for a distribution of electrons we need to integrate the single-electron emissivity against the distribution function over momentum space:

$$j_\nu = \int d^3p_e \frac{dN_e}{d^3p_e d^3x}\,\eta_\nu(\mathbf{p}_e), \tag{A1}$$

where $\mathbf{p}_e$ is the electron momentum. To evaluate j_ν, we need η_ν for an electron with nonzero momentum parallel to **B**, measured in the plasma rest frame. This can be calculated directly (see, e.g., Bekefi 1966). Here we start with the single-electron emissivity for an electron with zero momentum parallel to **B** and show explicitly that, by Lorentz boosts, one obtains the usual expression for the single-electron emissivity for an electron with nonzero momentum parallel to **B**. The emissivity of a distribution of electrons in frames other than the fluid (plasma center of momentum) frame can then be obtained using the Lorentz invariance of j_ν/ν^2.

Here is our strategy: identify the wavevector and electron four-momentum in the fluid frame (denoted [FF]), then transform these to a frame comoving with the electron's guiding center (denoted [GCF], and also denoted by primes), and use the resulting expressions for the photon wavevector and electron four-velocity to obtain η_ν in the guiding center frame. Finally, transform η_ν back to the fluid frame.

The photon wavevector is ($\omega = 2\pi\nu$)

$$k^\mu[\mathrm{FF}] = \{\omega, \omega\sin\theta, 0, \omega\cos\theta\} \tag{A2}$$

in a coordinate frame t, x, y, z. We assume, without loss of generality, that the wavevector lies in the x–z plane and the magnetic field is aligned with $\hat{z}$. The electron four-velocity is

$$u^\mu[\mathrm{FF}] = \{\gamma, \gamma\beta\sin\xi, 0, \gamma\beta\cos\xi\} \tag{A3}$$

where ξ is the electron pitch angle. As the time-averaged emission is invariant under rotations about $\hat{z}$, we have chosen an instant of time at which the electron's velocity is (spatially) coplanar with k^μ and the magnetic field.

Now we apply a Lorentz boost parallel to the magnetic field, transforming into the frame comoving with the electron guiding center:

$$\Lambda = \begin{pmatrix} \gamma_g & 0 & 0 & -\beta_g\gamma_g \\ 0 & 1 & 0 & 0 \\ 0 & 0 & 1 & 0 \\ -\beta_g\gamma_g & 0 & 0 & \gamma_g \end{pmatrix}, \tag{A4}$$

where β_g is the guiding center speed along the field line, which is $\beta\cos\xi$; the corresponding Lorentz factor is $\gamma_g^{-2} = 1 - \beta^2\cos^2\xi$.

The boosted wavevector is

$$k^\mu[\mathrm{GCF}] = \omega\{\gamma_g(1 - \beta_g\cos\theta), \sin\theta, 0, \gamma_g(\cos\theta - \beta_g)\} \tag{A5}$$

from which we deduce that

$$\nu' = \nu\gamma_g(1 - \beta_g\cos\theta) \tag{A6}$$

(the prime denotes the value in the [GCF]) and

$$\sin\theta' = \frac{\sin\theta}{\gamma_g(1 - \beta\cos\xi\cos\theta)} \tag{A7}$$

and

$$\cot^2\theta' = \gamma_g^2\left(\frac{\beta\cos\xi - \cos\theta}{\sin\theta}\right)^2. \tag{A8}$$

The boosted four-velocity is

$$u^\mu[\mathrm{GCF}] = \gamma\{\gamma_g(1 - \beta\beta_g\cos\xi), \beta\sin\xi, 0, 0\} \tag{A9}$$

from which we conclude that

$$\gamma' = \frac{\gamma}{\gamma_g} \tag{A10}$$

and

$$\beta' = \beta\gamma_g \sin\xi. \tag{A11}$$

In the guiding center frame the single-electron emissivity is (Schott 1912)

$$\eta_\nu[\mathrm{GCF}] \equiv \frac{dE'}{dt'd\Omega'd\nu'} = \frac{2\pi e^2\nu'^2}{c}\sum_{n=1}^{\infty}\delta(y_n')\left[\cot^2\theta' J_n^2(z) + \beta^2 J_n'^2(z)\right] \tag{A12}$$

where

$$y_n' \equiv \frac{n\nu_c}{\gamma'} - \nu', \tag{A13}$$

$$z = \frac{\nu'\beta'\gamma'}{\nu_c}\sin\theta', \tag{A14}$$

and $d\Omega'$ is the differential solid angle in [GCF].

We can evaluate all the arguments of η_ν[GCF] in terms of [FF]quantities:

$$y_n' = \frac{n\nu_c}{\gamma'} - \nu' = \gamma_g\left(\frac{n\nu_c}{\gamma} - \nu(1-\beta\cos\xi\cos\theta)\right) = \gamma_g y_n, \tag{A15}$$

since the field strength (and therefore ν_c) is the same in both frames and y_n is defined in Equation (16). Now,

$$\delta(y_n') = \delta(\gamma_g y_n) = \frac{1}{\gamma_g}\delta(y_n). \tag{A16}$$

Also (after substitution),

$$z = \frac{\nu'\beta'\gamma'}{\nu_c}\sin\theta' = \frac{\nu\beta\gamma}{\nu_c}\sin\theta\sin\xi, \tag{A17}$$

which recovers Equation (17). We have evaluated η_ν[GCF] in terms of quantities measured in the fluid frame:

$$\eta_\nu[\mathrm{GCF}] = \frac{2\pi e^2\nu'^2}{c}\sum_{n=1}^{\infty}\frac{1}{\gamma_g}\delta(y_n)\left[\gamma_g^2\left(\frac{\cos\theta-\beta\cos\xi}{\sin\theta}\right)^2 J_n^2(z) + \beta^2\sin^2\xi\,\gamma_g^2 J_n'^2(z)\right]; \tag{A18}$$

and we now need to find η_ν[FF].

Since

$$\eta_\nu = \frac{dE}{dtd\Omega d\nu} = h\nu^2\frac{dN}{\nu dtd\Omega d\nu}, \tag{A19}$$

and $\nu d\Omega d\nu$ and dN are invariant, then

$$\frac{\eta_\nu'}{\nu'^2}dt' = \frac{\eta_\nu}{\nu^2}dt. \tag{A20}$$

Since $dt'/dt = 1/\gamma_g$ (exercise for the reader), we are left with

$$\eta_\nu[\mathrm{FF}] = \frac{2\pi e^2\nu^2}{c}\sum_{n=1}^{\infty}\delta(y_n')\left[\left(\frac{\cos\theta-\beta\cos\xi}{\sin\theta}\right)^2 J_n^2(z) + \beta^2\sin^2\xi\, J_n'^2(z)\right], \tag{A21}$$

which is the usual expression, as given by Wardzinski & Zdziarski (2000) and Bekefi (1966), obtained by transformation rather than direct calculation.

APPENDIX B

EFFICIENT BESSEL FUNCTION CALCULATOR

In order to evaluate the accuracy of approximate formulae for the synchrotron emissivity we must compare them to the exact expression (31), which includes the Bessel function of the first kind $J_n(z)$ (Abramowitz & Stegun 1970). The function is a solution of the differential equation

$$\left[z^2\frac{d^2}{dz^2} + z\frac{d}{dz} + (z^2 - n^2)\right]J_n = 0 \tag{B1}$$

and has the series representation

$$J_n(z) = \left(\frac{z}{2}\right)^n\sum_{k=0}^{\infty}\frac{(-1)^k(z/2)^{2k}}{k!\,\Gamma(n+k+1)}. \tag{B2}$$

In our application, the order of the Bessel function is set by the resonance condition (16). Both z and n vary from 10^2 to $\sim 10^{13}$ for our target application (Noble et al. 2007). Since our evaluation of $j_\nu(\theta)$ requires us to evaluate a two-dimensional integral repeatedly, many evaluations of $J_n(z)$ are required. Further, the number of $J_n(z)$ calculations needed for the two-dimensional integral and the run-time per $J_n(z)$ evaluation using standard packages increases with ν/ν_c. This study therefore demanded we use an efficient $J_n(z)$ calculator accurate enough so that the final error in $j_\nu(\theta)$ is less than the error of our approximate expressions.

Facing the same computational hurdle as us, Chishtie et al. (2005)—who require large order calculations of $J_n(z)$ to high precision for Fourier transforming gravitational wave signals from pulsars—expanded further previously known approximate expansions for $J_n(z)$ in various limits. We demonstrate here for the first time that these expressions can be pieced together to form a continuous approximation for $J_n(z)$ up to $n \sim 10^{55}$. We do not use the more recent method described in Chishtie et al. (2008)—which is said to work over all limits in z/n—since it requires evaluating the Airy function and its derivative. The expressions given in Chishtie et al. (2005) satisfy our needs, were straightforward to implement, and relieved us from searching for a robust, efficient Airy function routine.

Our method uses three different approximate expansions, which we will call "Expansions 1–3," for three different domains: $z < n-d_1, z \sim n$, and $z > n+d_2$, where $d_{1,2}$ are functions of n given below. Expansions 1 and 3 use two-order extensions made by Chishtie et al. (2005) to expansions derived originally by Meissel (see Chishtie et al. 2005 for references to original works on the various series representations of $J_n(z)$). Specifically, we use Equations (10)–(12) of Chishtie et al. (2005) for Expansion 1, and Equations (12)–(14) of Chishtie et al. (2005) for Expansion 3. Expansion 2 is used in the so-called transition region, $z \sim n$, and is a five-term extension of Debye's "ϵ expansion" given in Equations (21) and (22) of Chishtie et al. (2005).

The extensions made by Chishtie et al. (2005) were essential for being able to match the expansions together for all n. We empirically found the locations—i.e., $z(n)$—at which an expansion starts to deviate by more than 0.1% from trusted values[5] over $100 < n < 10^7$. These locations $z(n)$ fit the

[5] The routine used to calculate the trusted values was the `jn` routine found in the GNU C compiler's math library (GNU Compiler Collection, http://gcc.gnu.org/).

Table 1
Routines for Evaluating the Bessel Function $J_n(z)$

Name	Reference	$n_{\max}$[a]
`my_Bessel_J`	This paper (Chishtie et al. 2005)	...
`bessjy`	Press et al. (1992)	10^{16}
`gsl_sf_bessel_Jn`	Galassi et al. (2006)	10^5
`jn`	GNU Compiler Collection	10^9
`s17dec`	NAG C Library[b]	10^9

Notes.
[a] $n_{\max}$ is the approximate maximum value of n a routine can calculate $J_n(n)$ to within 10% of the value from `my_Bessel_J`.
[b] The NAG C Library Mark 8, http://www.nag.co.uk/

following functions well:

$$z_- = n(1 - b_- n^{a_-}) \quad \text{for } z < n \tag{B3}$$

and

$$z_+ = n(1 - b_+ n^{a_+})^{-1} \quad \text{for } z > n, \tag{B4}$$

with $a_\pm$ and $b_\pm$ being different constants for each expansion. We found that each expansion's region of validity (to the 0.1% level) overlaps with another expansion's valid range, suggesting that at least one out of the three expansions is valid for any n, z. The boundaries dictating which expansion to use were finally chosen to be curves centered between neighboring methods' curves of validity. The curve marking the boundary between the first and second domains is

$$z_{12} = z_- : (a_-, b_-) \simeq (-0.66563, 1.8044) \tag{B5}$$

and the curve separating the second and third domains is

$$z_{23} = z_+ : (a_+, b_+) \simeq (-0.65430, 1.8708). \tag{B6}$$

One can show that, with 32 bit double-precision floating-point arithmetic, these curves are numerically indistinguishable from the curve $z = n$ for $n \gtrsim 10^{23}$; at these orders Expansion 2 is used only when $z = n$. For $n \gtrsim 10^{26}$, $J_n(z < n)$ is numerically equivalent to zero for any z numerically different from n since the function $J_n(z < n)$ becomes narrower as n increases. One may, however, resolve this issue by working in higher precision environments. Fortunately, our applications do not require us to do so since we are only interested in $n < 10^{14}$.

We have written a routine in the C programming language called `my_Bessel_J` that controls when to use which expansion and efficiently evaluates the appropriate expansion.[6] It has been extensively tested against a number of other routines, which we list in Table 1. All tests were performed on an Intel 3.06 GHz Xeon machine with the Intel C++ Compiler for Linux version 8.0 and the GNU C Compiler version 3.3.2.

Our first comparison attempts to measure the maximum value of n for which a routine can reliably calculate the Bessel function. In Table 1, we list the order of magnitude of n at which each method's evaluation of $J_n(n)$ begins to significantly deviate from our method's values. For small orders we are confident in our method since all methods agree with each other. At orders $n > 10^9$, however, only one other method is reliable (`bessjy`) and so the comparison is biased. At their limits, each method "fails" to return with a reasonable answer in different ways. Some return with obviously wrong values like $J_n(n) < 0$ (`gsl_sf_bessel_Jn` and `jn`), another reports that there is a loss of precision and returns with a null answer (`s17dec`), while the last reports that the calculation requires too many iterations and gives an inaccurate approximation (`bessjy`). Note that we are not confident in our method for $n > 10^{55}$ since this is when Expansion 2 evaluates $J_n(n) = 0$.

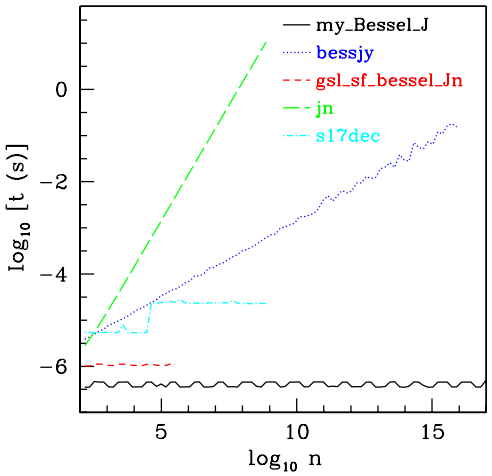

Figure 12. Logarithm of the time per $J_n(n)$ execution in seconds vs. n using the methods listed in Table 1. A method's execution time was only measured up to its $n_{\max}$. Note that the execution time of `my_Bessel_J` remains steady through $n = 10^{55}$; the plot was truncated for illustrative purposes.
(A color version of this figure is available in the online journal.)

This survey shows that there is an existing method, `bessjy`, that can reliably calculate $J_n(n)$ at orders well above our requirements. Unfortunately, as we see in Figure 12, it is costly and scales as a power law with n. `jn` has a steeper power-law scaling, while the others are practically independent of the Bessel function's order.[7] All but `gsl_sf_bessel_Jn` are significantly slower than our routine; `gsl_sf_bessel_Jn`, however, has the smallest domain of validity and cannot evaluate $J_n(z)$ at the values of n we need.

In Figure 13, we compare $J_n(z)$ at $n = 10^9$ to see how the three best methods compare with each other at large orders over a wide range in argument. The fact that `my_Bessel_J` agrees better with `s17dec` than does `bessjy` gives credence to our method. The imperfectness of the transitions from one expansion to another exhibits itself by narrow peaks in the relative error between `my_Bessel_J` and the other methods. These peaks lie immediately about the transition points, which are indicated by the dashed vertical lines. As z increases past n, round-off errors lead to significant phase errors. `my_Bessel_J` and `s17dec` both follow the asymptotically sinusoidal trend at large z, but `bessjy` eventually returns with 0 and indicates that it has reached its reliable limit.

To measure the accuracy at even larger orders, we employ the recurrence relation

$$\frac{2n}{z} J_n(z) = J_{n-1}(z) - J_{n+1}(z) \tag{B7}$$

and calculate the normalized deviation from it:

$$R_n(z) = \left| \frac{1}{J_n(z)} \left(\frac{2n}{z} J_n(z) - J_{n-1}(z) - J_{n+1}(z) \right) \right|, \tag{B8}$$

[6] Our routine and an example program are available to the public under the GNU Public License from the Web site at http://rainman.astro.illinois.edu/codelib/.

[7] The runtime for `s17dec` is constant up to $n \sim 10^4$, after which it is a larger constant.

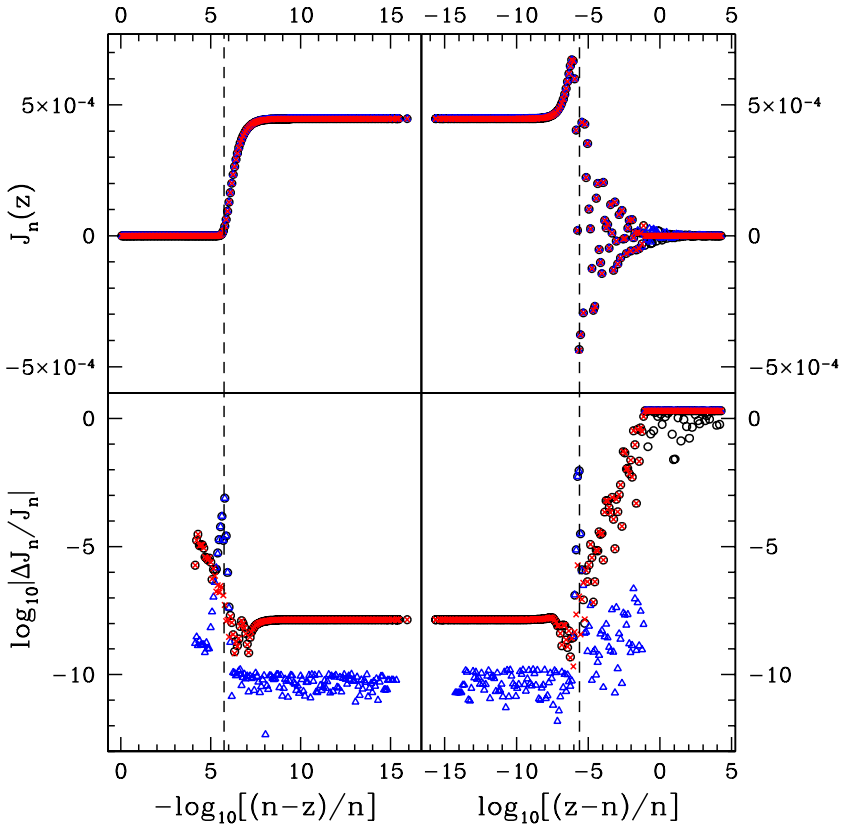

Figure 13. Comparison between $J_n(z)$ evaluations when $n = 10^9$. Top row: $J_n(z)$ using `my_Bessel_J` (circles), `bessjy` (triangles), and `s17dec` (x's). Bottom row: the logarithm of the relative error between `my_Bessel_J` and `bessjy` (circles), `my_Bessel_J` and `s17dec` (triangles), and `bessjy` and `s17dec` (x's). The plots on the left are shown for $z < n$, while those on the right are shown for $z > n$. The vertical dashed lines in the left and right plots indicate, respectively, z_- and z_+ at $n = 10^9$.

(A color version of this figure is available in the online journal.)

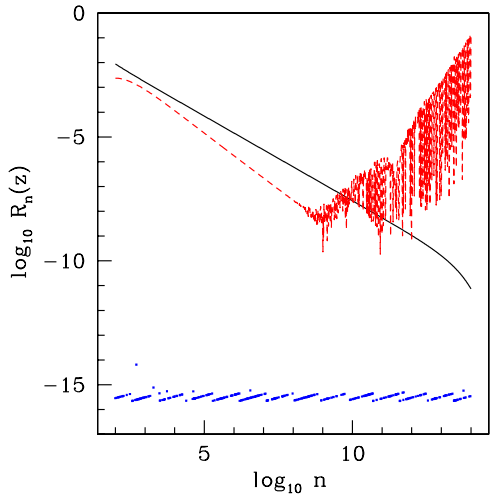

Figure 14. Logarithm of the normalized residual of the recurrence relation for $z = (1-\epsilon)z_-$ (solid curve), $z = n$ (squares), and $z = (1+\epsilon)z_+$ (dashes), which—respectively—use expansions 1–3, where $\epsilon = 10^{-13}$. Please see Equation (B8) for the definition of $R_n(z)$.

(A color version of this figure is available in the online journal.)

which should be identically zero. We calculate $R_n(z)$ for three different arguments over a wide range of n in Figure 14. Each curve uses one of the three expansions. The errors in Expansions 1 and 3 both diminish with n, except when round-off errors lead to significant phase errors in Expansion 3 for $n \gtrsim 10^8$. Expansion 2, however, always satisfies the recurrence relation to within 32 bit double precision for all n. For even higher orders $n \to 10^{55}$, we have made sure that `my_Bessel_J` satisfies the well-known upper bounds (Abramowitz & Stegun 1970):

$$J_n(n) < \frac{[2/(9n)]^{1/3}}{\Gamma(2/3)}, \quad |J_n(z)| \leqslant \frac{(z/2)^n}{\Gamma(n+1)}, \quad \text{and}$$
$$|J_n(n\epsilon)| \leqslant \left| \frac{\epsilon^n \exp\left[n\sqrt{1-\epsilon^2}\right]}{(1+\sqrt{1-\epsilon^2})^n} \right|. \tag{B9}$$

REFERENCES

Abramowitz, M., & Stegun, I. A. 1970, Handbook of Mathematical Functions (New York: Wiley)
Bekefi, G. 1966, Radiation Processes in Plasmas (New York: Wiley)
Blumenthal, G. R., & Gould, R. J. 1970, Rev. Mod. Phys., 42, 237
Brainerd, J. J., & Lamb, D. Q. 1987, ApJ, 313, 231
Brainerd, J. J., & Petrosian, V. 1987, ApJ, 320, 703
Chanmugam, G., Barrett, P. E., Wu, K., & Courtney, M. W. 1989, ApJS, 71, 323
Chishtie, F. A., Rao, K. M., Kotsireas, I. S., & Valluri, S. R. 2008, Int. J. Mod. Phys. D, 17, 1197
Chishtie, F. A., Valluri, S. R., Rao, K. M., Sikorski, D., & Williams, T. 2005, in Proc. 19th Annu. Int. Symp. on High Performance Computing Systems and Applications (HPCS 2005), ed. I. S. Kotsireas & D. Stacy (Guelph, Canada: IEEE Computer Society), 34
Crusius, A., & Schlickeiser, R. 1986, A&A, 164, L16
Crusius, A., & Schlickeiser, R. 1988, A&A, 196, 327
Dulk, G. A. 1985, ARA&A, 23, 169
Fleishman, G. D., & Melnikov, V. F. 2003, ApJ, 584, 1071

Galassi, M., Davies, J., Theiler, J., Gough, B., Jungman, G., Booth, M., & Rossi, F. 2006, GNU Scientific Library Reference Manual (2nd ed.; Boston: Free Software Foundation), http://www.gnu.org/software/gsl/
Ginzburg, V. L. 1970, The Propagation of Electromagnetic Waves in Plasmas (2nd ed.; Oxford: Pergamon)
Ginzburg, V. L., & Syrovatskii, S. I. 1968, Ap&SS, 1, 442
Kawabata, K. 1964, PASJ, 16, 30
Mahadevan, R., Narayan, R., & Yi, I. 1996, ApJ, 465, 327
Marcowith, A., & Malzac, J. 2003, A&A, 409, 9
Meggitt, S. M. A., & Wickramasinghe, D. T. 1982, MNRAS, 198, 71
Melia, F. 1994, ApJ, 426, 577
Melrose, D. B. 1989, Instabilities in Space and Laboratory Plasmas (Cambridge: Cambridge Univ. Press)
Melrose, D. B., & McPhedran, R. C. 1991, Electromagnetic Processes in Dispersive Media (Cambridge: Cambridge Univ. Press)
Noble, S. C., Leung, P. K., Gammie, C. F., & Book, L. G. 2007, Class. Quantum Grav., 24, 259
Pacholczyk, A. G. 1970, Radio Astrophysics: Nonthermal Processes in Galactic and Extragalactic Sources (San Francisco, CA: Freeman)
Petrosian, V. 1981, ApJ, 251, 727
Petrosian, V., & McTiernan, J. M. 1983, Phys. Fluids, 26, 3028
Press, W. H., Teukolsky, S. A., Vetterling, W. T., & Flannery, B. P. 1992, Numerical Recipes in C: The Art of Scientific Computing (Cambridge: Cambridge Univ. Press)
Robinson, P. A., & Melrose, D. B. 1984, Aust. J. Phys., 37, 675
Rybicki, G. B., & Lightman, A. P. 1979, Radiative Processes in Astrophysics (New York: Wiley)
Scheuer, P. A. G. 1968, ApJ, 151, L139
Schlickeiser, R., & Lerche, I. 2007, A&A, 476, 1
Schott, G. A. 1912, Electromagnetic Radiation (Cambridge: Cambridge Univ. Press)
Stix, T. H. 1992, Waves in Plasmas (New York: AIP)
Takahara, F., & Tsuruta, S. 1982, Prog. Theor. Phys., 67, 485
Väth, H. M., & Chanmugam, G. 1995, ApJS, 98, 295
Wardzinski, G., & Zdziarski, A. 2000, MNRAS, 314, 183
Westfold, K. C. 1959, ApJ, 130, 241
Wolfe, B., & Melia, F. 2006, ApJ, 637, 313